Desmosome mutations impact the tumor microenvironment to promote melanoma proliferation

Maayan Baron[1], Mohita Tagore[2], Patrick Wall[1], Fan Zheng[1], Dalia Barkley[3], Itai Yanai[3], Jing Yang[4], Maija Kiuru[5], Richard M. White[2] , Trey Ideker[1,6]

[1] Department of Medicine, University of California San Diego, La Jolla, CA USA
[2] Cancer Biology and Genetics, Memorial Sloan Kettering Cancer Center, New York, NY USA
[3] Institute for Computational Medicine, NYU School of Medicine, New York, NY USA
[4] Department of Pharmacology, University of California San Diego, La Jolla, CA USA
[5] Depts. of Dermatology and Pathology, University of California Davis, Sacramento, CA USA
[6] Department of Bioengineering, University of California San Diego, La Jolla, CA USA

Correspondence to T.I. (tideker@ucsd.edu)

Keywords:
Cancer, Melanoma, Melanocytes, Keratinocytes, Genetics, Genomics, Desmosome, Microenvironment, Tumor Evolution, Single-Cell RNA Sequencing, Spatial Transcriptomics, Co-culture

Desmosomes are transmembrane protein complexes that contribute to cell-cell adhesion in epithelia and other tissues. Here, we report the discovery of frequent genetic alterations in the desmosome in human cancers, with the strongest signal seen in cutaneous melanoma where desmosomes are mutated in over 70% of cases. In primary but not metastatic melanoma biopsies, the burden of coding mutations on desmosome genes associates with a strong reduction in desmosome gene expression. Analysis by spatial transcriptomics suggests that these expression decreases occur in keratinocytes in the microenvironment rather than in primary melanoma tumor cells. In further support of a microenvironmental origin, we find that loss-of-function knockdowns of the desmosome in keratinocytes yield markedly increased proliferation of adjacent melanocytes in keratinocyte/melanocyte co-cultures. Thus, gradual accumulation of desmosome mutations in neighboring cells may prime melanocytes for neoplastic transformation.

Transformation of melanocytes to skin cutaneous melanoma (SKCM) includes interaction with numerous cells in the tumor microenvironment which can play important roles in progression[1,2]. One important component of this microenvironment is the keratinocyte, which forms the major cellular component of the epidermis, the top layer of skin. Nascent melanoma cells detach from neighboring keratinocytes, regulating melanocyte homeostasis through paracrine signaling and cell-cell adhesion[3–9] and impacting tumor proliferation and invasion.

A primary adhesion structure that facilitates the physical interaction between melanocytes and keratinocytes is the desmosome, an intercellular junction conserved across vertebrates[10]. Desmosomes have a transmembrane core composed of cadherin proteins (desmogleins and desmocollins) which is linked via plakoglobin and plakophilin proteins to keratin filaments in the cytoplasm[11] (Fig. 1a). Alterations to desmosome components can impair tissue strength and have been documented to have both positive and negative effects on cell proliferation and differentiation[12]. For example, increases in expression of desmosome cadherins can stimulate release of plakoglobin followed by increased Wnt/β-catenin signaling, and overexpression of plakophilin 3 (PKP3) has been associated with poor patient survival and advanced disease stage in non-small cell lung carcinomas[13]. In contrast, upregulation of plakoglobin has been found to suppress cell proliferation in bladder cancer cells *in vitro*[14,15].

While these studies have focused on desmosome expression, a separate question is whether the desmosome is impacted by genetic mutations. Recently, we performed an integrative analysis of protein biophysical interactions and tumor mutations[16], resulting in a map of 395 protein complexes under mutational selection in one or more cancer types. One of these complexes pointed to the desmosome as a potential focal point for accumulation of mutations in

melanoma; however, at the time we did not validate or further explore this observation (Supplementary Fig. 1).

Here, to investigate the importance of mutations to the desmosome complex, we began with a comprehensive survey of somatic non-synonymous mutations impacting any of the 13 desmosome genes in aggregate, across 32 tumor tissue types profiled by The Cancer Genome Atlas (TCGA). By far the highest mutation recurrence was observed for skin cutaneous melanoma (SKCM), in which 71% of tumors harbored a desmosome coding mutation. In contrast, desmosome mutation rates were substantially lower in all other tissue types (<40%, Fig. 1b).

Since melanomas are one of the tumor types with generally high genome-wide burden of mutations[17], we sought to assess the significance of desmosome mutation rates in several ways. First, we computed the excess mutational load on the 13 desmosome genes using MutSigCV[17], which takes into account the genome-wide mutation burden, the type of mutational signature(s)[18], and gene-specific factors such as mRNA expression level and time of replication during cell cycle. We found that as a group, desmosome genes are mutated significantly more often than expected, again with the strongest signal in melanoma (Fig. 1c). Second, we repeated this analysis in an independent melanoma cohort[19], again finding that desmosome genes are highly and significantly mutated (Supplementary Fig. 2). These patterns did not depend on the particular mutational model for expected mutational frequency ($P < 10^{-20}$ using MutSigCV[17] and $P < 10^{-9}$ using oncodriveFML[20]). Third, ranking human genes by decreasing mutation frequency in melanoma, we found that all 13 desmosome genes were among the top quartile, on par with the distribution of well-established melanoma cancer genes (Fig. 1d).

Notably, none of the desmosome genes had been previously reported to be significantly mutated in melanoma when analyzed individually[17,19,21], perhaps since the mutational signal is spread across the desmosome complex.

The finding that the desmosome is frequently mutated in melanoma was puzzling, since in normal epidermis, desmosome function has been typically associated with keratinocytes rather than melanocytes[22]. However, this is a point of some confusion, since melanocytes cultured in the absence of other cell types have been shown to express the desmosomal cadherin Dsg2[23,24] leading to increased migration[25]. To more fully understand the patterns and cell types associated with desmosome expression in melanoma tumors, we performed single-cell RNA sequencing (scRNA-seq) on two human primary melanoma tumor biopsies encapsulating approximately 1,000 cells from each tumor using the inDrop system[26,27] (Fig. 2a). Single-cell transcriptomes were displayed using UMAP[28] (Uniform Manifold Approximation and Projection) resulting in clusters that matched pre-identified distinct cell types (Online Methods). Analysis against a panel of established RNA markers for different human cell types distinguished clear populations of immune, epithelial, muscle, keratinocyte and melanocyte tumor types (Fig. 2b). Examining the expression profile of desmosome genes across these different types, we found desmosomes to be predominantly expressed in keratinocytes (Fig. 2c-d). This analysis was corroborated by published datasets of human metastatic melanoma[29] and primary transgenic zebrafish tumors[30], in which we also found that desmosome expression is limited to keratinocytes (Supplementary Fig. 3).

To investigate the relationship between desmosome expression and mutation, we next examined multi-omics data collected from 472 melanoma tumors (104 primary and 368

metastatic) by TCGA[31]. Analysis of these data indicated that the expression of the desmosome system was significantly higher in primary than metastatic tumors (Fig. 3a). Examining the matched somatic mutation data, we found that primary tumors with desmosome mutations had significantly reduced expression of the desmosome complex in comparison to tumors without such mutations (Fig. 3b). Moreover, in primary melanoma only, there was a strong inverse relationship between the number of desmosome genes that are mutated in a tumor and overall desmosome expression (Fig. 3c). Examining previously collected melanoma transcriptional profiles[29,32,33], we found that, in primary melanoma tumors, desmosome mutation associates with significantly higher expression of genes related to cell proliferation (Fig. 3d). To determine if these particular mutations are under evolutionary selection pressure, we calculated the ratio of nonsynonymous to synonymous mutations (dN/dS)[34] in the desmosome genes. We found that dN/dS was approximately 2.5 in primary melanoma tumors, indicating strong positive selection, and that this value was significantly larger than for metastatic melanoma tumors (Fig. 3e). These results suggested that accumulation of mutations in the desmosome disrupt its expression in a graded manner, and that these events are selected in primary, but not metastatic, melanoma.

We reasoned that the distinction between primary and metastatic melanoma could be due to at least two explanations. First was the very different microenvironments of these two tumor locales. Primary melanoma tumor biopsies tend to contain large numbers of surrounding keratinocytes due to their growth within and below the epidermis, in contrast to metastatic tumors which, apart from cutaneous metastases, lack the epidermal component and are typically purer[35]. In this case, the decrease in desmosome expression could be due to loss of desmosomal expression in keratinocytes. A second explanation was related to cancer-specific transcriptional states of melanocytes. Since melanoma tumors can assume distinct

transcriptional programs[29,33,36], the effect on desmosome expression could be due to a change in transcriptional state of melanocytes between primary and metastatic cancer.

To distinguish between these two possibilities, we performed a spatial transcriptomics analysis on primary tumor biopsies drawn from a cohort of eight melanoma patients. Samples were first characterized by bulk whole-exome sequencing, identifying three tumors with desmosome mutations and five without (Fig. 4a, Supplementary Table 1). Paraffin-embedded sections of each tumor were stained using specific markers to identify cancer melanocytes (S100B marker), keratinocytes (pan-cytokeratin marker), or immune cells (CD45 marker). Using these markers, 48 regions of interest (ROIs, 4-8 per tumor × 8 tumors) were selected to enrich for melanocytes, keratinocytes or a combination of both cell types (Fig. 4b). We then used the NanoString GeoMx Spatial Profiler[37] to measure the mRNA expression of 18,695 genes in each ROI.

Analysis of the spatial RNA data showed that the expression profiles of ROIs were well-clustered according to cell type and desmosome expression levels (Supplementary Fig. 4). Desmosome expression was very high in keratinocyte-enriched ROIs but barely detectable in melanocyte-enriched ROIs (Fig. 4c), corroborating our earlier findings with scRNA-seq (Fig. 2b-c). Moreover, desmosome expression in keratinocyte ROIs was significantly lower in tumors with desmosome mutations than in tumors lacking such mutations (Fig. 4d, $P<0.05$). In contrast, we did not see substantial change in desmosome expression in melanocyte ROIs when comparing mutated versus unmutated samples (Fig. 4d). Therefore, the spatial profiling data supported a model in which desmosome mutation leads to a reduction in desmosome expression specifically in keratinocytes.

We next examined whether such loss of desmosome expression in keratinocytes could influence the behavior of neighboring melanocyte tumor cells. For this purpose, we created a keratinocyte cell line (HaCaT human immortalized keratinocytes, Online Methods) and subjected this line to transient knockdown of the desmoplakin gene using small interfering RNAs (*DSP* siRNAs, Supplementary Table 3). We chose to knockdown *DSP* since, out of all desmosome-encoding genes, it was the one that had been shown previously to effectively disrupt desmosome structure[38], and it also had the single largest mutation burden in melanoma patients (Fig. 1c-d). After confirming that *DSP* gene expression was significantly reduced by siRNA knockdown (Supplementary Fig. 5, Online Methods), we examined the effect on cell proliferation. For this purpose we characterized growth of both melanocytes and keratinocytes, in both monoculture and co-culture conditions (Fig. 5a). In monocultures, *DSP* knockdown led to a decrease in proliferation in keratinocytes but not in melanoma cells (Supplementary Fig. 6). In contrast, when melanocytes and keratinocytes were grown together in co-culture, we found that proliferation of melanoma cells increased by more than two-fold upon *DSP* knockdown in keratinocytes (Fig. 5b). These results indicated that loss of desmosome expression in keratinocytes can promote neighboring melanocyte growth (Fig. 5c).

Typically, studies of the cancer genome have focused on identifying frequent genetic alterations in single genes, or associations between individual gene alterations and tumor functional outcomes[39–42]. The main challenge of these gene-by-gene approaches is that most cancer mutations are rare. However, consideration of groups of genes, corresponding to discrete cellular components such as protein complexes and signaling pathways, provides an expanded means of understanding mutational effects[16,43–45]. Using such a strategy we have shown that the desmosome complex is frequently impacted by coding mutations in primary melanoma samples,

associated with a substantial decrease in expression of desmosome components. Spatial transcriptomic profiling indicates these expression decreases occur predominantly in keratinocytes in the tumor local microenvironment rather than in melanocyte tumor cells. These observations are corroborated by genetic disruptions showing that loss of the DSP desmosome subunit in keratinocytes has the effect of amplifying the proliferation of adjacent melanocytes in co-culture.

The observed interplay between keratinocytes and melanocytes stands in contrast to the usual mode by which somatic mutations are thought to promote cancer, by direct selection in a clonal population of tumor cells. Our results are however consistent with earlier findings that non-tumor cells can indeed carry cancer-causing mutations, predominantly in genes associated with tumor initiation rather than clonal expansion[46–48]. For example, a study of melanocyte transformation identified that non-tumor cells close to a melanoma tumor have significantly greater numbers of mutations than those farther away, including mutations in oncogenes such as *BRAF*[49]. Our findings not only support the notion that tumors arise from a collection of cells rather than a clonal population[50–53], but they extend that notion to other cell types which are not necessarily the cell type of origin. By such a model, mutations in complementary cellular communities may alter expression programs and growth profiles which, in turn, help determine the order in which specific mutations arise within the complex cancer tissue.

Online Methods:

Statistical framework for desmosome enrichment. The enrichment of coding mutations in the desmosome system was computed for each TCGA cancer cohort, as follows. We first used the MutSigCV software[17] to calculate the number of tumor samples expected to show mutations for each desmosome gene, assuming that gene was not under positive selection. In deriving this expectation, MutSigCV takes into account the local mutational signatures, DNA replication time and mRNA expression level relevant to the gene in question. Next, we computed the difference between this expected mutation count and the actual count of tumors for which that gene had somatic coding mutations. Genes were sorted in decreasing order of (observed – expected) mutation counts. In order to calculate significance, a bootstrapping approach was applied; Briefly, the average ranks of the desmosome genes were then compared to 100,000 permuted lists to produce a p-value for each TCGA cancer cohort. P-values were corrected for multiple hypothesis testing using Benjamani-Hochberg procedure to yield Q-values.

Single-cell RNA sequencing of primary melanoma tumors. Melanoma tumors were collected post-operatively from two patients who consented and signed 604 IRB. To obtain single-cell suspensions, samples were washed in PBS and cut into small pieces (4-5 mm^3) followed by dissociation using the Miltenyi human tumor dissociation kit according to manufacturer instructions. Red blood cells were depleted using ACK lysis buffer for 3 minutes. Dead cells were removed, if needed, using the Milyenty dead cell separator. Single cell encapsulation and library preparation were performed using the inDrop platform[26,27] followed by sequencing on an Illumina NextSeq. Sequencing reads were de-multiplexed, aligned and counted using a custom pipeline as described previously[33] to produce a raw count matrix for each tumor. Quality control was also performed as described previously[54]. The raw matrix count was first transformed to

UMIs (Unique Molecular Identifiers) to correct for library preparation duplications[55]. Cells with >750 distinct UMIs, mitochondrial transcripts <20% and ribosomal transcripts <30% were selected for analysis. UMI counts for the selected cells were normalized by the total number of transcripts per cell, and a scale factor equivalent to the median number of transcripts across all cells was applied (transcripts per median, TPM). Expression was transformed using the Freeman-Tukey transform as described previously[56].

UMAP 2D projection and annotation of single-cell mRNA-seq data. We selected genes with both above-mean mRNA expression level and above-mean Fano factor (a standardized measure of variance). These genes were then used as features to project cells onto two dimensions using the Uniform Manifold Approximation and Projection for Dimension Reduction (UMAP) technique with default parameters[28]. Ten communities of cells were clearly discernible in the resulting UMAP projection (Fig. 2b,c). To label the cell type represented by each community, we identified the top differentially expressed genes in each ($p < 10^{-6}$, Kolmogorov Smirnov test; effect size > 0.2, Cohen's d). These genes were cross-referenced against a collection of published gene expression markers of known cell types[29,30,36,57,58], allowing unambiguous assignment of each community to one of five types: immune (markers: *CD45*, *CD4*, *CD8A*), epithelial (*EPCAM*), muscle (*MYH11*), melanocyte (*SOX10*, *SOX2*, *S100B*) or keratinocyte (*KRT4*, *KRT5*, *KRT17*, *KRT19*). To further annotate a subset of melanocytes as malignant, we inferred copy-number variations (CNV) from the RNA-seq profiles with inferCNV[59], using all other cells from the same tumor sample as a reference. All three melanocyte communities were found to have a common pattern of aneuploidy in their CNV profiles, indicating cancer.

Spatial transcriptomics by GeoMX platform. Formalin-fixed paraffin-embedded (FFPE) samples of eight primary melanomas were chosen and sectioned (clinical information provided in Supplementary Table 2). Three sections were taken from each tumor: two were processed for whole-exome sequencing to determine desmosome mutation status, and one was retained for the digital spatial profiling workflow to determine desmosome expression. Digital spatial profiling was performed using the GeoMX system as previously described[60]. Immunofluorescent visualization markers for keratinocytes (*PanCK*), melanocytes (*S100B*, *PMEL*) and immune cells (*CD45*) were used to guide the selection of regions of interest (ROIs) containing either pure or mixed areas of each cell type (keratinocyte, melanocyte) followed by RNA profiling using the GeoMx human whole assay.

DSP functional assays. For desmoplakin (*DSP*) knockdown studies we used Dharmacon ON-TARGETplus SMARTpool siRNAs (n = 4 distinct *DSP*-targeting siRNAs, n = 4 non-targeting control siRNAs, Supplementary Table 3), with cells treated according to manufacturer instructions. Briefly, melanoma (A375) or keratinocyte (HaCaT) cell types were seeded overnight in regular media with no antibiotics in six-well dishes as monocultures. Cells were then transfected with either *DSP*-targeting or non-targeting control siRNA pools along with DharmaFECT 1 transfection reagent (Horizon #T-2005-01) in serum-free media. After 72 hours, siRNA-treated cells were administered a second dose of siRNA followed by a 48-hour incubation. *DSP* knockdown efficiency was measured using qPCR (Supplementary Fig. 5). Cells treated with *DSP* siRNAs (melanoma or keratinocyte) were then co-cultured with the opposite cell type treated with non-targeting control siRNA (keratinocyte or melanoma). Melanoma cells and keratinocytes were plated in a 1:5 ratio and incubated for 48 hours, then harvested prior to confluency.

A375/HaCaT phospho-histone H3 (pH3) immunostaining. Cells were fixed in 4% PFA and stained simultaneously using the following antibodies: phospho-histone H3 primary antibody (1:1000; Millipore #05-806); anti-human SOX10 (ThermoFisher #PA5-84795); anti-human KRT17 conjugated to Alexa Fluor 546 (Santa Cruz Biotechnology #sc-393002 AF546). Cells were placed overnight at 4ºC and then counterstained with AlexaFluor 647 anti-mouse IgG (Cell Signaling #4410), after which >10 images per condition were acquired in a Zeiss AxioObserver fluorescence microscope. The number of mitotic cells was quantified by calculating double-positive cells (SOX10+, AlexaFluor647+ or KRT17+, AlexaFluor647+) as a fraction of the total number of SOX10+ or KRT17+ cells in each field. To quantify cells, 2000 or 5000 cells/well (melanoma cells or keratinocytes) were plated in a 96-well plate followed by 72-96 hour incubation. Proliferation was measured using the Cyquant Cell Proliferation assay as per manufacturer instructions. Fluorescence was read using a BioTek Synergy 96-well plate reader, with all values normalized to the control conditions.

Data Availability:

All 'omics datasets relevant to this study will be deposited to relevant public databases upon acceptance of this article for publication. Principal 'omics datasets are:

Dataset	Database	Accession Number
Single-cell RNA sequencing of primary melanoma tumors	Gene Expression Omnibus	TBD
Spatial transcriptomics by GeoMX platform	Gene Expression Omnibus	TBD

Code Availability:

All code used for this work, including custom algorithms and analysis scripts, has been distributed on GitHub at the URL: http://github.com/MaayanBaron/desmosome_paper.git.

Author Contributions:

M.B. and T.I. conceived and implemented the study, M.T., M.B. and R.W. designed and performed the functional work. D.B. M.B. and I.Y. performed and analyzed the single cell RNA-Seq work. M.B., T.I. and M.K. performed and analyzed the Spatial Transcriptomics work. F.Z., P.W. and J.Y. provided critical interpretation. The paper was written by M.B. and T.I. and was critically reviewed and approved by all of the coauthors.

Declaration of Interests:

T.I. is a co-founder, member of the advisory board, and has an equity interest in Data4Cure and Serinus Biosciences. T.I. is a consultant for and has an equity interest in Ideaya BioSciences. The terms of these arrangements have been reviewed and approved by UC San Diego in accordance with its conflict of interest policies. R.M.W. is a paid consultant to N-of-One, a subsidiary of Qiagen.

Acknowledgements:

We gratefully acknowledge funding support from the National Institutes of Health under grants NCI U54 CA274502 and NIGMS P41 GM103504 to T.I.

Figures:

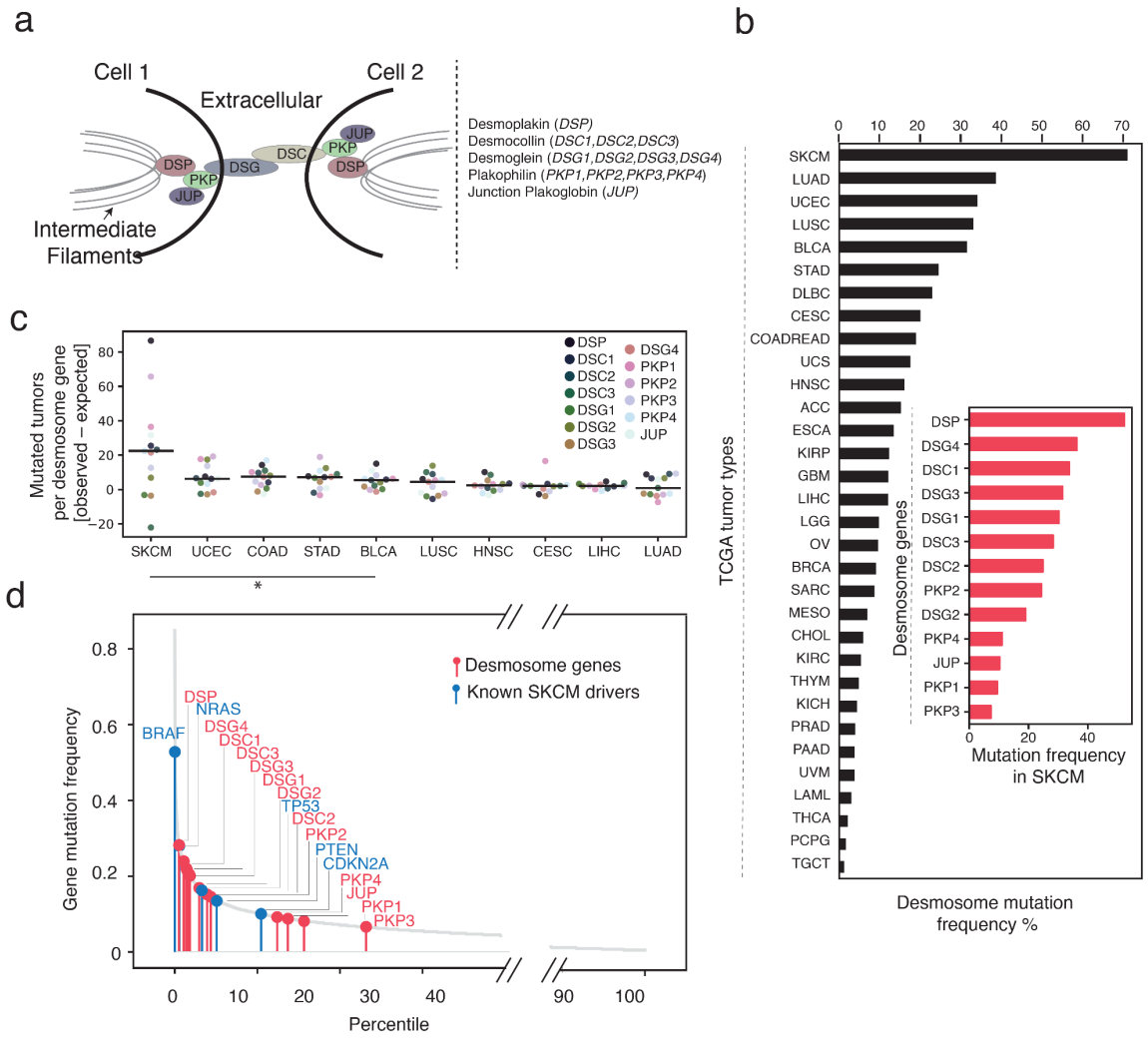

Fig. 1: The desmosome system and its patterns of mutation.

(a) Illustration of the desmosome complex, which is composed of proteins of three different families: cadherins (*DSG*s and *DSC*s), armadillo proteins (*PKP*s and *JUP*) and the plakin protein desmoplakin (*DSP*).

(b) Desmosome mutation frequency for each of 32 tumor types, with mutations aggregated across the 13 desmosome genes. Inset: Mutation frequency of each desmosome gene in skin cutaneous melanoma (SKCM). Other cancer type abbreviations: ACC - Adrenocortical carcinoma (n = 92), BLCA - Bladder urothelial carcinoma (n = 413), BRCA - Breast invasive carcinoma (n = 1108), CESC - Cervical squamous cell carcinoma and endocervical adenocarcinoma (n = 310), CHOL - Cholangiocarcinoma (n = 51), COADREAD - Colorectal adenocarcinoma (n = 640), DLBC - Lymphoid neoplasm diffuse large B cell lymphoma (n = 48), ESCA - Esophageal carcinoma (n = 186), GBM - Glioblastoma multiforme (n = 619), HNSC - Head and neck squamous cell carcinoma (n = 530), KICH - Kidney chromophobe (n = 113), KIRC - Kidney renal clear cell carcinoma (n = 538), KIRP - Kidney renal papillary cell carcinoma (n = 293), LAML - Acute myeloid leukemia (n = 200), LGG - Brain lower grade glioma (n = 530), LIHC - Liver hepatocellular carcinoma (n = 442), LUAD - Lung adenocarcinoma (n = 586), LUSC - Lung squamous cell carcinoma (n = 511), MESO - Mesothelioma (n = 87), OV - Ovarian serous cystadenocarcinoma (n = 617), PAAD - Pancreatic adenocarcinoma (n = 186), PCPG - Pheochromocytoma and paraganglioma (n = 184), PRAD - Prostate adenocarcinoma

(n = 501), SARC - Sarcoma (n = 265), STAD - Stomach adenocarcinoma (n = 478), TGCT - Testicular germ cell tumors (n = 156), THCA - Thyroid carcinoma (n = 516), THYM - Thymoma (n = 124), UCEC - Uterine corpus endometrial carcinoma (n = 549), UCS - Uterine carcinosarcoma (n = 57), UVM - Uveal melanoma (n = 80).

(c) Excess number of tumors with a mutated desmosome gene (colored points) above the number expected by chance (Online Methods). Horizontal black line indicates median value across desmosomal genes. Top ten most frequently mutated tumor types from (b) are shown. Significance determined using bootstrap analysis (*, q-value<10^{-10}, Benjamani-Hochberg correction for multiple testing).

(d) Ranked SKCM mutation frequencies of each human gene. Desmosome genes, red; known SKCM driver genes[22], blue.

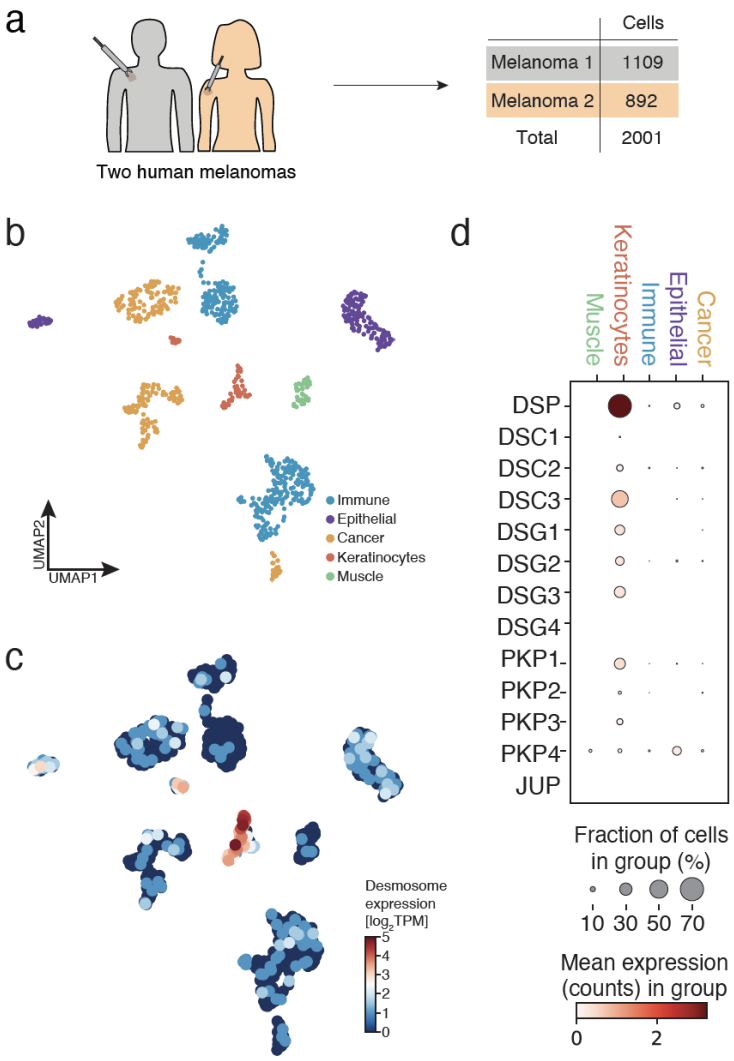

Fig. 2: Single-cell analysis of desmosome gene expression in human melanomas.

(a) Tumor biopsies from two patients, one male and one female, processed using scRNA-Seq.

(b) Uniform Manifold Approximation and Projection (UMAP) analysis of 1109 individual cells from Melanoma 1, with color indicating inferred cell type. “Cancer” denotes melanoma cells.

(c) Same UMAP as (b), with color indicating the expression of desmosome genes in transcripts per median (TPM, Online Methods).

(d) Correspondence of desmosome gene expression to cell types. Color indicates mean expression per cell ($\log_2$). Point size indicates fraction of cells in cell type expressing each desmosome gene.

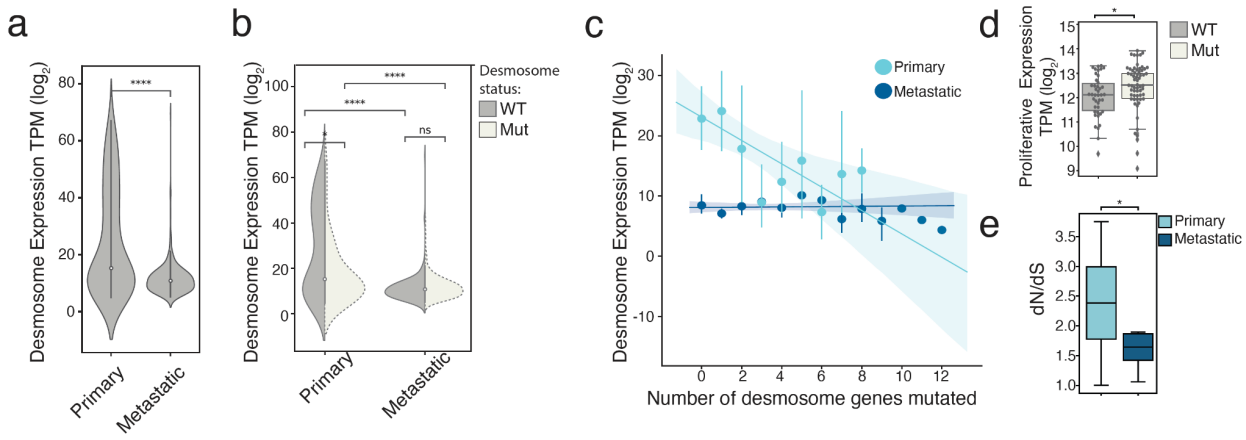

Fig. 3: Relationship of desmosome expression to tumor grade and mutational status.

(a) Violin plot of average desmosome gene expression in primary (left, n = 104) or metastatic (right, n = 362) melanoma tumors in TCGA. Significance determined by two sample t-test (****, $P<10^{-4}$). TPM, transcripts per median.

(b) Same as (a) distinguishing wild-type (WT, gray) and desmosome-mutated (white, n = 62 for primary tumors, n = 277 for metastatic tumors) tumors in the TCGA cohort. Significance determined by two sample t-test (****, $P<10^{-4}$; *, $P<0.05$; ns, not significant).

(c) Average desmosome gene expression (TPM) as a function of the number of desmosome genes with coding mutations. Shown separately for primary (light blue) versus metastatic (dark blue) melanoma tumor populations. Regression lines for each of these populations are shown: Primary melanoma, slope = –0.66; metastatic melanoma, slope = 0.03; significant difference with $P<0.01$. Error bars represent standard deviation and the shaded areas capture 95% confidence intervals.

(d) Degree of proliferative gene expression (defined previously[32]) in desmosome WT (gray, n = 42) or desmosome mutant (white, n = 62) primary melanoma tumors (points) in the TCGA cohort. Significance determined by two sample t-test (*, $P<0.05$). The boxes in the plot contain the 25th to 75th percentile, the middle line denotes the 50th percentile, and the whiskers mark the 5th and 95th percentiles.

(e) Ratio of fixed nonsynonymous-to-synonymous mutations (dN/dS) in primary (light blue, n = 12 genes across 104 patients) or metastatic (dark blue, n = 12 genes across 362 patients) melanoma tumors in the TCGA cohort. The distributions of dN/dS across the population of tumors are shown by box plots, using similar display convention to panel d. Significance determined by two sample t-test (*, $P<0.05$).

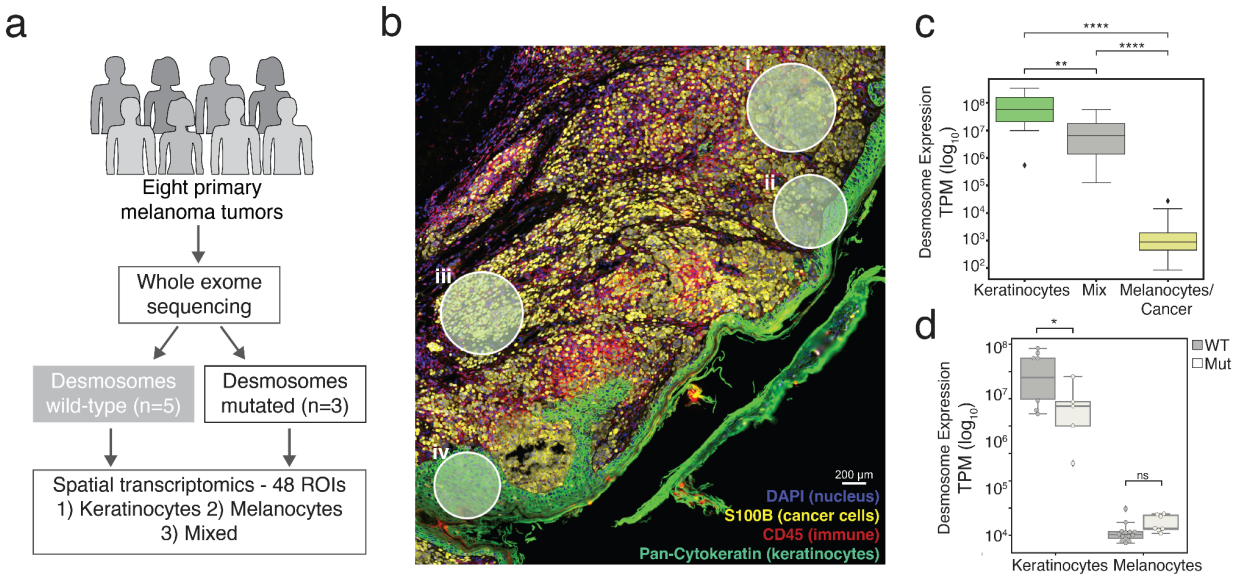

Fig. 4: Spatial transcriptomics of tumors with mutated or wild-type desmosomes.

(a) Eight primary melanoma tumors were processed using whole exome sequencing and digital spatial profiling to characterize a total of 48 regions of interest (ROIs).

(b) Example ROIs (roman numerals) enriched for melanocytes (i,iii), mixed melanocytes and keratinocytes (ii), or keratinocytes (iv), overlayed on image. Fluorescent markers label nuclei (blue), cancer cells (yellow), immune cells (red), or keratinocytes (green).

(c) Average mRNA expression levels of desmosome genes in each ROI, stratified by keratinocyte (green, n = 15), mix (gray, n = 12) or melanocyte (yellow, n = 21) ROIs. In the boxplots, lower and upper box boundaries delineate the 25th and 75th percentiles, the middle line denotes the 50th percentile, and whiskers mark the 5th and 95th percentiles. Significance determined by two sample t-test (**** $P<10^{-4}$, ** $P<10^{-2}$).

(d) Average mRNA expression levels of desmosome genes in each ROI, stratified by keratinocytes (left, n = 15) and melanocytes (right, n = 21) and further subdivided based on whether ROIs are from tumors with wild-type (WT, dark gray, n = 10 for keratinocytes and n = 14 for melanocytes) or mutant desmosomes (light gray, n = 5 for keratinocytes and n = 7 for melanocytes). Within each category the set of ROI values is summarized by box plot, following the convention of panel c. Significance determined by two sample t-test (*, P<0.05, ns, not significant).

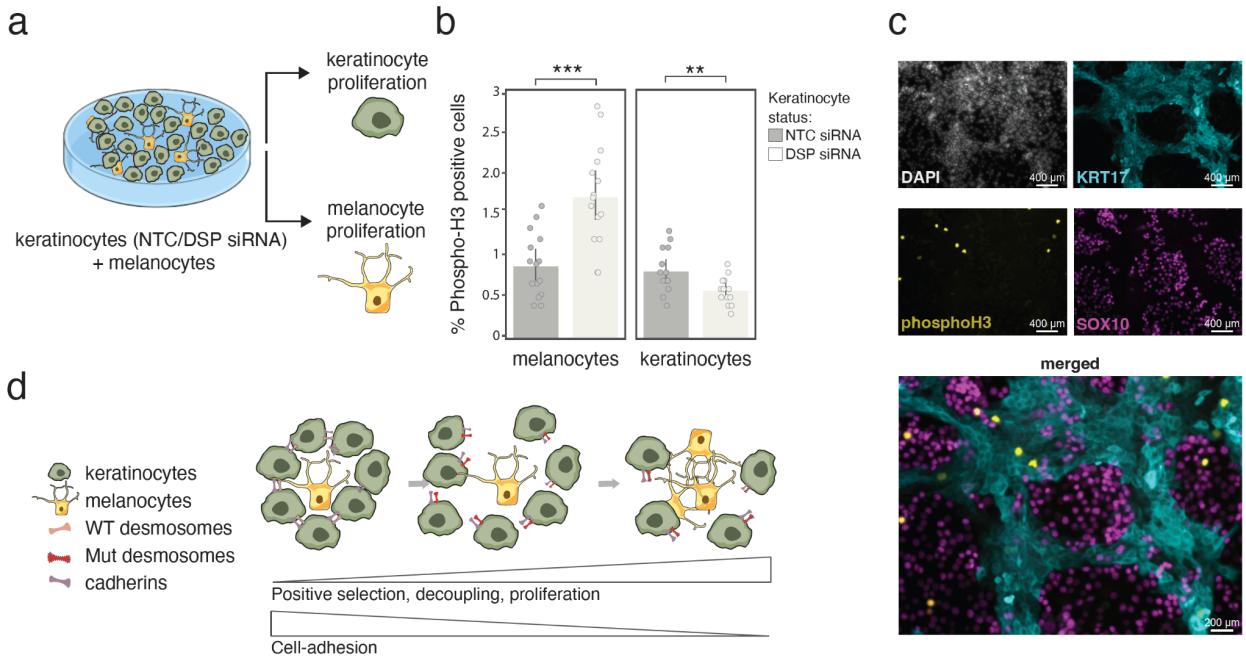

Fig. 5: Effects of *DSP* gene disruption in melanoma-keratinocyte co-cultures.

(a) Schematic of co-culture experiment. To generate the data shown in subsequent figure panels (b,c), melanoma cells were co-cultured with keratinocytes exposed to either non-targeting control (NTC) siRNA or *DSP* siRNA gene disruptions. Cell-type populations were isolated and characterized by phospho-H3 cell proliferation assay.

(b) Phospho-H3 assay of melanocyte (left) versus keratinocyte (right) cell proliferation, shown for co-cultures in which keratinocytes were treated with NTC siRNA (dark gray) versus *DSP* siRNA (light gray). Each bar summarizes 5 distinct wells × 3 biological replicates for n = 15 replicate co-culture measurements. *** P<0.001, ** P<0.01. Error bars represent 95% confidence intervals.

(c) Representative co-culture images staining keratinocytes (cyan, KRT17 marker), melanocytes (purple, SOX10 marker), and proliferating cells (yellow, phosphoH3 readout). White color reflects all cell nuclei (DAPI). Images correspond to the NTC experiment.

(d) Suggested model in which desmosome mutations in keratinocytes lead to keratinocyte-melanocyte decoupling and decreased keratinocyte adhesion which, in turn, promote melanocyte proliferation.

Supplementary Table 1: Number of missense variants detected in eight melanoma tumors. Related to Fig. 4.

	Missense Variants
MKD1	16
MKD6	15
MKD5	14
MKD4	12
MKD7	10
MKD3	8
MKD2	7
MKD8	6

Supplementary Table 2: Clinical information on the eight melanoma tumors.
Related to Fig. 4.

Tumor ID	Age	Sex	Tumor site	Tumor thickness	Mitotic rate
MKD1	40	M	Back	1.0 mm	1 / mm^2
MKD2	61	M	Back	1.1 mm	2 / mm^2
MKD3	75	M	Left arm	0.9 mm	5 / mm^2
MKD4	60	M	Back	2.1 mm	>10 / mm^2
MKD5	86	F	Right shoulder	0.7 mm	0 / mm^2
MKD6	56	M	Back	0.5 mm	1 / mm^2
MKD7	54	F	Right arm	0.9 mm	2 / mm^2
MKD8	84	F	Chest	3.4 mm	8 / mm^2

Supplementary Table 3: *DSP* siRNA sequences.
Related to Fig. 5.

siRNA ID	Target Sequence
siRNA A-019800-13, DSP	GCUCCAUGGUAGAAGAUAU
siRNA A-019800-14, DSP	UCACUGAGCUAGUAGAUUC
siRNA A-019800-15, DSP	CGAUGUACUUGUUUGGUUU
siRNA A-019800-16, DSP	CGAUGUACUUUAAGGUGUC

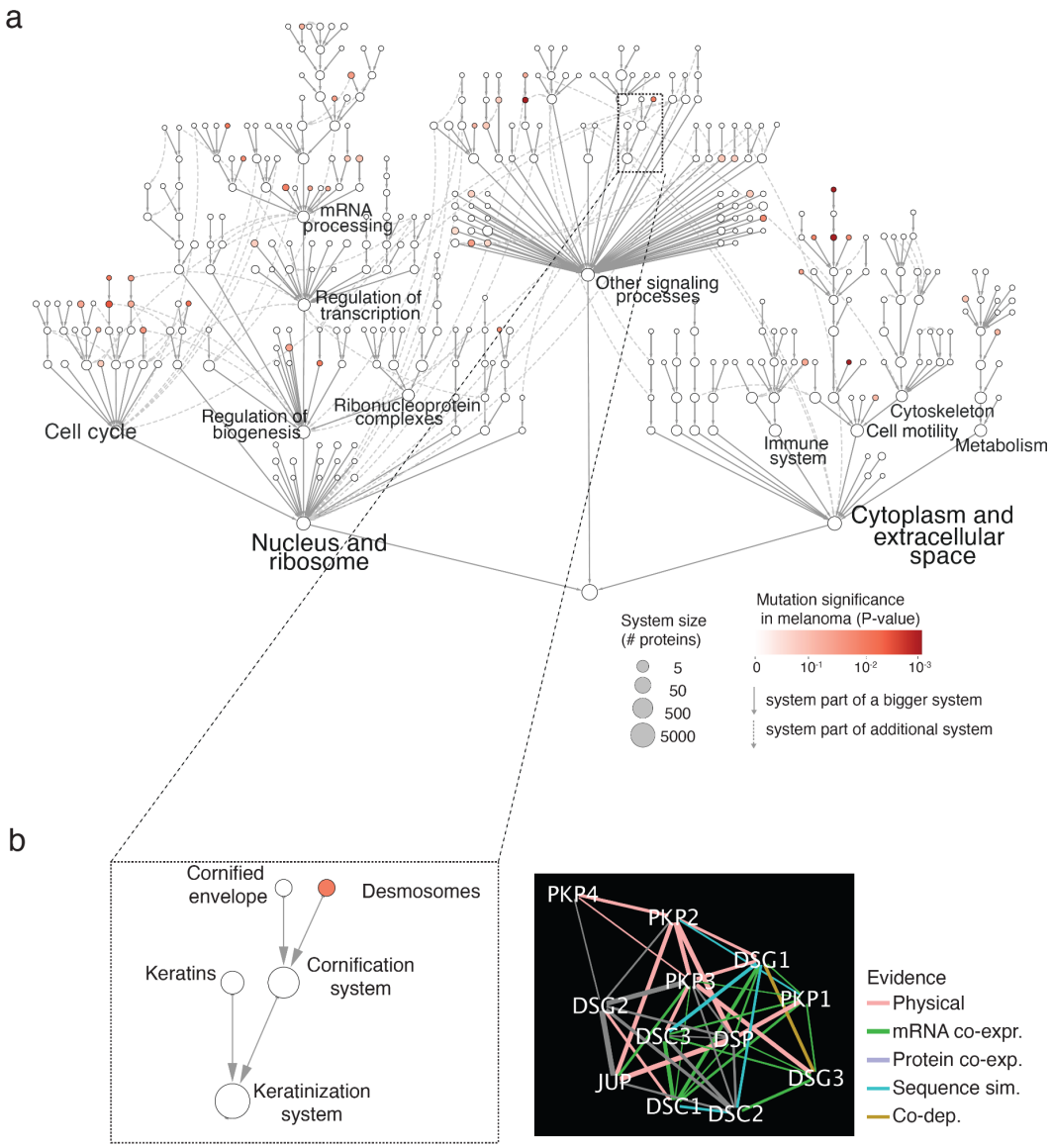

Supplementary Fig. 1: Interactions defining desmosome system and context in NeST hierarchy.

(a) Nested Systems in Tumors (NeST) map showing all mutated systems identified across TCGA cohorts, published previously[16]. Nodes represent protein systems, identified in the previous study from dense communities of interacting proteins. Node size indicates the size of the system in number of proteins. Red intensity scale indicates significance of system mutation frequency in the skin cutaneous melanoma (SKCM) cohort. Gray arrows represent hierarchical containment (i.e. system 1 → system 2 denotes that system 1 is contained by system 2). For systems contained by multiple others (pleiotropy), each additional containment relation is connected by a dashed arrow.

(b) Zoom detail of NeST hierarchy relevant to the desmosome system and its larger containing compartments (left). Adjacent is the specific protein interaction network that defines the desmosome system (right). Colors denote interaction types: Red: physical protein-protein interactions; green: correlation in mRNA expression; purple: correlation in protein abundance; cyan: protein sequence similarity; brown: co-dependency interactions, connecting proteins for which loss-of-function gene knockouts result in similar patterns of growth dependency across cell lines. See original publication[16] for more details.

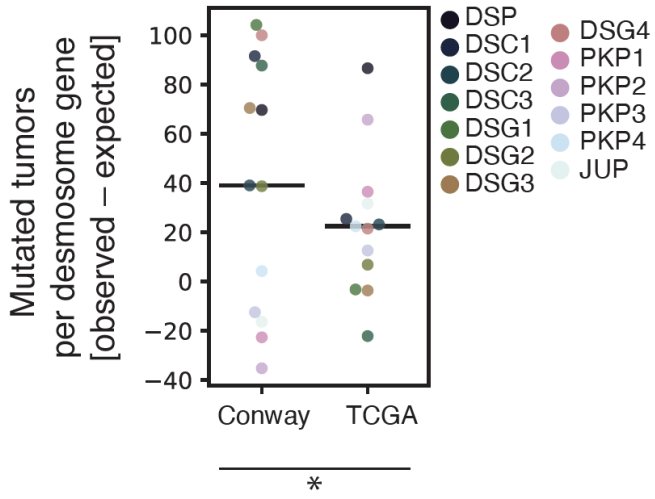

Supplementary Fig. 2: Desmosome mutation frequencies in multiple melanoma cohorts. Counts of mutated tumors per each desmosome gene (colored points) in the largest published melanoma cohort (Conway[19], left) compared to the SKCM-TCGA cohort (right). Significance determined using bootstrap analysis (*, $P<10^{-10}$). Related to Fig. 1.

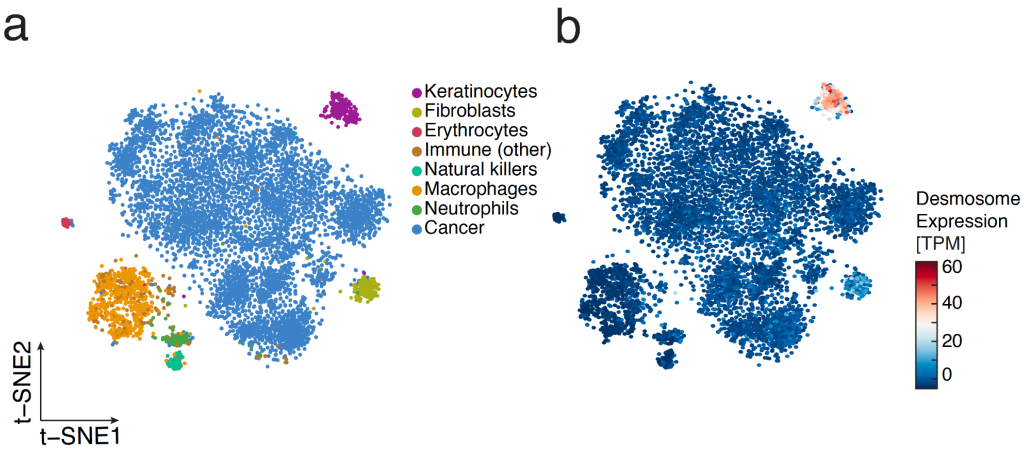

Supplementary Fig. 3: Single-cell RNA sequencing analysis of melanoma samples.
Shows desmosomes are expressed predominantly in keratinocytes rather than melanocytes in zebrafish primary tumors. Related to Fig. 2.

(a) t-distributed stochastic neighbor embedding (tSNE) analysis of approximately 7500 individual cells from zebrafish melanoma cells. Reanalysis of data published previously[33]. Color indicates inferred cell type.

(b) Same tSNE plot as panel (a), colored by the expression of desmosome genes.

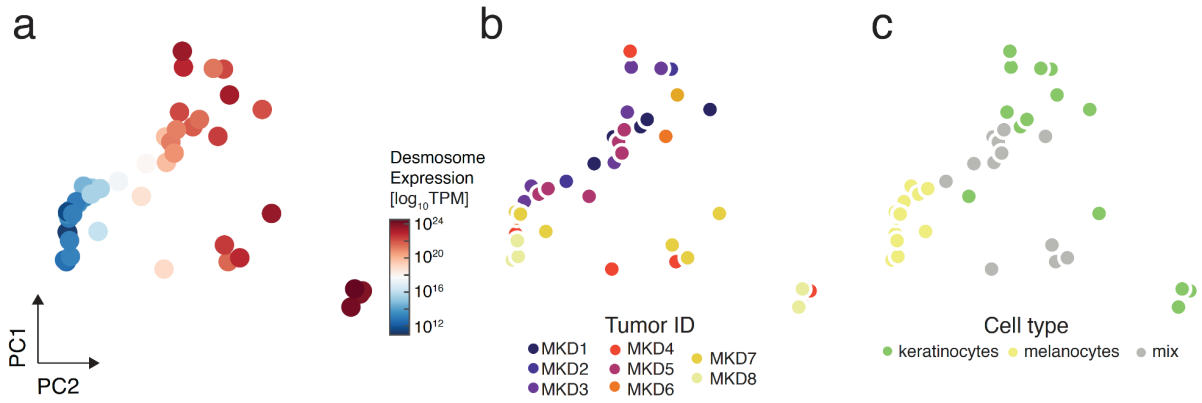

Supplementary Fig. 4: Principal Component Analysis (PCA) of spatial transcriptomic data.
Related to Fig. 4.

(a) Profiles of mRNA expression for each ROI (covering 18,695 genes total) are reduced to the first two principal components (PC1 versus PC2). A total of 48 ROIs are drawn from 8 tumor biopsies. Color indicates average expression of desmosome genes.
(b) Same PCA as (a), color indicates tumor ID.
(c) Same PCA as (a), color indicates cell type identified by antibody staining.

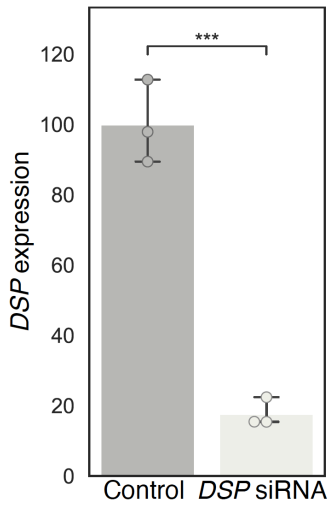

Supplementary Fig. 5: Quantitative PCR assay of *DSP* expression. *DSP* relative expression level after treatment of keratinocytes with *DSP* siRNA (light gray, right, n = 3 replicates) versus NTC siRNA (dark gray, left, n = 3 replicates). Significance determined based on two sample t-test (***, P<0.001). Related to Fig. 5.

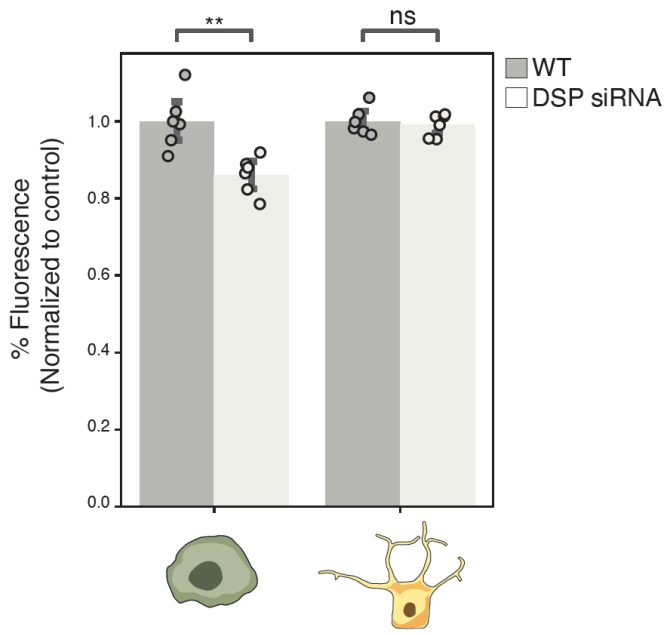

Supplementary Fig. 6: Proliferation assay in monocultures. Proliferation of keratinocytes (left) or melanocytes (right), using non-targeting control siRNA (dark gray) or *DSP* siRNAs (light gray). Significance based on two sample t-test (n = 6 replicates, **, P<0.01; ns, not significant). Related to Fig. 5.

References:

1. Hanahan, D. & Weinberg, R. A. Hallmarks of cancer: the next generation. *Cell* **144**, 646–674 (2011).

2. Chen, F. *et al.* New horizons in tumor microenvironment biology: challenges and opportunities. *BMC Med.* **13**, 45 (2015).

3. Kim, I. S. *et al.* Microenvironment-derived factors driving metastatic plasticity in melanoma. *Nat. Commun.* **8**, 14343 (2017).

4. Kunisada, T. *et al.* Keratinocyte expression of transgenic hepatocyte growth factor affects melanocyte development, leading to dermal melanocytosis. *Mech. Dev.* **94**, 67–78 (2000).

5. Chung, H., Suh, E.-K., Han, I.-O. & Oh, E.-S. Keratinocyte-derived laminin-332 promotes adhesion and migration in melanocytes and melanoma. *J. Biol. Chem.* **286**, 13438–13447 (2011).

6. Haass, N. K. & Herlyn, M. Normal human melanocyte homeostasis as a paradigm for understanding melanoma. *J. Investig. Dermatol. Symp. Proc.* **10**, 153–163 (2005).

7. Hsu, M.-Y. *et al.* E-Cadherin Expression in Melanoma Cells Restores Keratinocyte-Mediated Growth Control and Down-Regulates Expression of Invasion-Related Adhesion Receptors. *Am. J. Pathol.* **156**, 1515–1525 (2000).

8. Shih, I. M., Elder, D. E., Hsu, M. Y. & Herlyn, M. Regulation of Mel-CAM/MUC18 expression on melanocytes of different stages of tumor progression by normal keratinocytes. *Am. J. Pathol.* **145**, 837–845 (1994).

9. Ableser, M. J., Penuela, S., Lee, J., Shao, Q. & Laird, D. W. Connexin43 reduces melanoma growth within a keratinocyte microenvironment and during tumorigenesis in vivo. *J. Biol. Chem.* **289**, 1592–1603 (2014).

10. Green, K. J., Jaiganesh, A. & Broussard, J. A. Desmosomes: Essential contributors to an integrated intercellular junction network. *F1000Research* vol. 8 2150 Preprint at https://doi.org/10.12688/f1000research.20942.1 (2019).

11. Garcia, M. A. & Nelson, W. J. Cell–cell junctions organize structural and signaling networks. *Cold Spring Harbor* (2018).

12. Chidgey, M. & Dawson, C. Desmosomes: a role in cancer? *Br. J. Cancer* **96**, 1783–1787 (2007).

13. Furukawa, C. *et al.* Plakophilin 3 oncogene as prognostic marker and therapeutic target for lung cancer. *Cancer Res.* **65**, 7102–7110 (2005).

14. Rieger-Christ, K. M. *et al.* Restoration of plakoglobin expression in bladder carcinoma cell lines suppresses cell migration and tumorigenic potential. *Br. J. Cancer* **92**, 2153–2159 (2005).

15. Canes, D. *et al.* Histone deacetylase inhibitors upregulate plakoglobin expression in bladder carcinoma cells and display antineoplastic activityin vitro andin vivo. *International Journal of Cancer* vol. 113 841–848 Preprint at https://doi.org/10.1002/ijc.20634 (2005).

16. Zheng, F. *et al.* Interpretation of cancer mutations using a multiscale map of protein systems. *Science* **374**, eabf3067 (2021).

17. Lawrence, M. S. *et al.* Mutational heterogeneity in cancer and the search for new cancer-associated genes. *Nature* **499**, 214–218 (2013).

18. Alexandrov, L. B. *et al.* The repertoire of mutational signatures in human cancer. *Nature* **578**, 94–101

(2020).

19. Conway, J. R. *et al.* Integrated molecular drivers coordinate biological and clinical states in melanoma. *Nat. Genet.* **52**, 1373–1383 (2020).

20. Mularoni, L., Sabarinathan, R., Deu-Pons, J., Gonzalez-Perez, A. & López-Bigas, N. OncodriveFML: a general framework to identify coding and non-coding regions with cancer driver mutations. *Genome Biol.* **17**, 128 (2016).

21. Hayward, N. K. *et al.* Whole-genome landscapes of major melanoma subtypes. *Nature* **545**, 175–180 (2017).

22. Barbieri, J. S., Wanat, K. & Seykora, J. Skin: Basic Structure and Function. *Pathobiology of Human Disease* 1134–1144 Preprint at https://doi.org/10.1016/b978-0-12-386456-7.03501-2 (2014).

23. Rickelt, S. *et al.* Subtypes of melanocytes and melanoma cells distinguished by their intercellular contacts: heterotypic adherens junctions, adhesive associations, and dispersed desmoglein 2 glycoproteins. *Cell and Tissue Research* vol. 334 401–422 Preprint at https://doi.org/10.1007/s00441-008-0704-7 (2008).

24. Schmitt, C. J. *et al.* Homo- and Heterotypic Cell Contacts in Malignant Melanoma Cells and Desmoglein 2 as a Novel Solitary Surface Glycoprotein. *Journal of Investigative Dermatology* vol. 127 2191–2206 Preprint at https://doi.org/10.1038/sj.jid.5700849 (2007).

25. Peitsch, W. K. *et al.* Desmoglein 2 depletion leads to increased migration and upregulation of the chemoattractant secretoneurin in melanoma cells. *PLoS One* **9**, e89491 (2014).

26. Zilionis, R. *et al.* Single-cell barcoding and sequencing using droplet microfluidics. *Nat. Protoc.* **12**, 44–73 (2017).

27. Klein, A. M. *et al.* Droplet barcoding for single-cell transcriptomics applied to embryonic stem cells. *Cell* **161**, 1187–1201 (2015).

28. McInnes, L., Healy, J., Saul, N. & Großberger, L. UMAP: Uniform Manifold Approximation and Projection. *Journal of Open Source Software* vol. 3 861 Preprint at https://doi.org/10.21105/joss.00861 (2018).

29. Tirosh, I. *et al.* Dissecting the multicellular ecosystem of metastatic melanoma by single-cell RNA-seq. *Science* **352**, 189–196 (2016).

30. Baron, M. *et al.* The Stress-Like Cancer Cell State Is a Consistent Component of Tumorigenesis. *Cell Syst* **11**, 536–546.e7 (2020).

31. Cancer Genome Atlas Network. Genomic Classification of Cutaneous Melanoma. *Cell* **161**, 1681–1696 (2015).

32. Hoek, K. S. *et al.* In vivo switching of human melanoma cells between proliferative and invasive states. *Cancer Res.* **68**, 650–656 (2008).

33. Baron, M. *et al.* A population of stress-like cancer cells in melanoma promotes tumorigenesis and confers drug resistance. *bioRxiv* 396622 (2020) doi:10.1101/396622.

34. Mugal, C. F., Wolf, J. B. W. & Kaj, I. Why time matters: codon evolution and the temporal dynamics of dN/dS. *Mol. Biol. Evol.* **31**, 212–231 (2014).

35. Aran, D., Sirota, M. & Butte, A. J. Corrigendum: Systematic pan-cancer analysis of tumour purity.

Nat. Commun. **7**, 10707 (2016).

36. Jerby-Arnon, L. *et al.* A Cancer Cell Program Promotes T Cell Exclusion and Resistance to Checkpoint Blockade. *Cell* **175**, 984–997.e24 (2018).

37. Beechem, J. M. High-Plex Spatially Resolved RNA and Protein Detection Using Digital Spatial Profiling: A Technology Designed for Immuno-oncology Biomarker Discovery and Translational Research. in *Biomarkers for Immunotherapy of Cancer: Methods and Protocols* (eds. Thurin, M., Cesano, A. & Marincola, F. M.) 563–583 (Springer New York, 2020).

38. Wanuske, M.-T. *et al.* Clustering of desmosomal cadherins by desmoplakin is essential for cell-cell adhesion. *Acta Physiol.* **231**, e13609 (2021).

39. Network, T. C. G. A. R. & The Cancer Genome Atlas Research Network. Comprehensive genomic characterization defines human glioblastoma genes and core pathways. *Nature* vol. 455 1061–1068 Preprint at https://doi.org/10.1038/nature07385 (2008).

40. Stransky, N. *et al.* The mutational landscape of head and neck squamous cell carcinoma. *Science* **333**, 1157–1160 (2011).

41. Wang, L. *et al.* SF3B1 and other novel cancer genes in chronic lymphocytic leukemia. *N. Engl. J. Med.* **365**, 2497–2506 (2011).

42. Morin, R. D. *et al.* Frequent mutation of histone-modifying genes in non-Hodgkin lymphoma. *Nature* **476**, 298–303 (2011).

43. Hofree, M., Shen, J. P., Carter, H., Gross, A. & Ideker, T. Network-based stratification of tumor mutations. *Nat. Methods* **10**, 1108–1115 (2013).

44. Olcina, M. M. *et al.* Mutations in an Innate Immunity Pathway Are Associated with Poor Overall Survival Outcomes and Hypoxic Signaling in Cancer. *Cell Reports* vol. 25 3721–3732.e6 Preprint at https://doi.org/10.1016/j.celrep.2018.11.093 (2018).

45. Leiserson, M. D. M. *et al.* Pan-cancer network analysis identifies combinations of rare somatic mutations across pathways and protein complexes. *Nat. Genet.* **47**, 106–114 (2015).

46. Kakiuchi, N. & Ogawa, S. Clonal expansion in non-cancer tissues. *Nat. Rev. Cancer* **21**, 239–256 (2021).

47. Jaiswal, S. *et al.* Age-related clonal hematopoiesis associated with adverse outcomes. *N. Engl. J. Med.* **371**, 2488–2498 (2014).

48. Martincorena, I. *et al.* Tumor evolution. High burden and pervasive positive selection of somatic mutations in normal human skin. *Science* **348**, 880–886 (2015).

49. Tang, J. *et al.* The genomic landscapes of individual melanocytes from human skin. *Nature* **586**, 600–605 (2020).

50. McGranahan, N. & Swanton, C. Clonal Heterogeneity and Tumor Evolution: Past, Present, and the Future. *Cell* **168**, 613–628 (2017).

51. Batlle, E. & Clevers, H. Cancer stem cells revisited. *Nat. Med.* **23**, 1124–1134 (2017).

52. Shah, S. P. *et al.* The clonal and mutational evolution spectrum of primary triple-negative breast cancers. *Nature* **486**, 395–399 (2012).

53. Sottoriva, A. *et al.* A Big Bang model of human colorectal tumor growth. *Nat. Genet.* **47**, 209–216

(2015).

54. Baron, M. *et al.* A Single-Cell Transcriptomic Map of the Human and Mouse Pancreas Reveals Inter- and Intra-cell Population Structure. *Cell Syst* **3**, 346–360.e4 (2016).

55. Grün, D. & van Oudenaarden, A. Design and Analysis of Single-Cell Sequencing Experiments. *Cell* **163**, 799–810 (2015).

56. Wagner, F., Yan, Y. & Yanai, I. K-nearest neighbor smoothing for high-throughput single-cell RNA-Seq data. *bioRxiv* (2017).

57. Nieto, P. *et al.* A single-cell tumor immune atlas for precision oncology. *Genome Res.* **31**, 1913–1926 (2021).

58. Barkley, D. *et al.* Cancer cell states recur across tumor types and form specific interactions with the tumor microenvironment. *Nat. Genet.* **54**, 1192–1201 (2022).

59. inferCNV of the Trinity CTAT Project. https://github.com/broadinstitute/inferCNV.

60. Merritt, C. R. *et al.* Multiplex digital spatial profiling of proteins and RNA in fixed tissue. *Nat. Biotechnol.* **38**, 586–599 (2020).